

<https://doi.org/10.1038/s44407-026-00055-8>

Photochemical ozone formation oriented VOC source apportionment and health economic burdens in Pearl River Delta

Check for updates

Weiqliang Deng^{1,2}, Lu Wang^{1,2,3}, Jin Huang^{1,2}, Zhizhao Guo^{1,2}, Jinghong Yang^{1,2}, Jukun Xiong^{1,2}, Hongli Liu^{1,2} & Meicheng Wen^{1,2}✉

Clarifying the source apportionment of volatile organic compounds (VOCs) and their correlation with photochemical losses and ozone formation is critically important. However, addressing this issue remains a significant challenge. To address this challenge, we proposed a novel photochemical ozone formation potential (PL-OFP)-oriented source apportionment method that facilitates the quantitative evaluation of VOC source contributions to ozone formation and associated health-economic burdens in the Pearl River Delta (PRD) urban agglomeration. Our findings indicate that PL-OFP values in the urban agglomeration ranged from 18.4 to 34.4 ppbv. Alkenes and aromatics were the dominant loss species because their unsaturated bonds are more susceptible to free-radical attack. Although natural gas and biomass combustion were the highest-concentration sources of VOCs, vehicle emissions had the greatest potential to form ozone. Notably, after photochemical reaction, over 70% of VOCs from biological sources were consumed, making them the dominant actual ozone contributor. Control measures should therefore prioritize these low-concentration but highly reactive VOC emissions. By quantifying health-economic burdens, it was estimated that the PRD region had 8522 O₃-related mortalities annually, resulting in economic losses of \$4933.4 M. Among these losses, PL-VOCs contributed \$1195.6 M. This research offers critical insights for the synergistic control of VOC and ozone.

Volatile organic compounds (VOCs) are a class of readily volatilized compounds at 50–260 °C, characterized by varied carbon skeleton structures and physicochemical properties¹. As key precursors for the formation of ozone (O₃) and secondary organic aerosol (SOA), VOCs undergo photochemical oxidation reactions with atmospheric oxidants such as hydroxyl radicals (•OH), and nitrogen oxides (NO_x)². VOCs can directly or indirectly influence air quality (such as O₃, PM_{2.5}), climate change, and human health through photochemical reactions³. Due to the wide variety and complex sources of VOCs, their atmospheric behavior exhibits significant variability⁴. The atmospheric lifetime, transport, and transformation of VOCs are significantly influenced by their physicochemical properties, particularly their chemical reactivity.

O₃ is a hazardous atmospheric pollutant involved in photochemical smog formation, posing increased health risks to humans. It attacks

carbon-carbon double bonds in unsaturated fatty acids within the human body, damaging lipids in cell membranes, and generating harmful peroxidation products such as intracellular peroxisomal fatty acid β-oxidase⁵ and 9-HpODE⁶, thus accelerating diseases like atherosclerosis. Previous studies have demonstrated that each 10 μg m⁻³ increment in O₃ concentration elevates all-cause mortality by 3.7%, cardiovascular mortality by 3.9%, and respiratory mortality by 5.0%⁷. However, during the warm season in China, O₃ concentration has been increasing at an annual rate of 5%^{8,9}. The Pearl River Delta (PRD), one of the most important economic areas in China, has implemented measures to control emissions of O₃ and VOCs¹⁰. Despite these control measures, O₃ concentrations have continued to increase by 2.1% annually over the past decade⁴. O₃ has not been effectively controlled. If there is no effective control policy for O₃ in the future, O₃ will lead to higher health-economic burdens¹¹. Therefore, the

¹Guangdong Key Laboratory of Environmental Catalysis and Health Risk Control, Guangdong-Hong Kong-Macao Joint Laboratory for Contaminants Exposure and Health, Institute of Environmental Health and Pollution Control, Guangdong University of Technology, Guangzhou, China. ²Guangdong Engineering Technology Research Center for Photocatalytic Technology Integration and Equipment, Guangzhou Key Laboratory of Environmental Catalysis and Pollution Control, School of Environmental Science and Engineering, Guangdong University of Technology, Guangzhou, China. ³School of Biology and Food Engineering, Guangdong University of Education, Guangzhou, China. ✉e-mail: meicheng.wen@gdut.edu.cn

implementation of effective policies to control ambient O_3 concentrations is urgently needed.

Atmospheric oxidation of VOCs is a key pathway driving photochemical O_3 formation (Fig. 1). Under sunlight irradiation, VOCs undergo hydroxyl radical ($\bullet OH$) initiated chain reactions, generating peroxy radicals ($RO_2\bullet$, $HO_2\bullet$), these radicals oxidize NO to NO_2 , ultimately leading to O_3 formation through NO_2 photolysis¹². Recent studies have found a positive correlation between atmospheric VOC and O_3 in the PRD region¹³ and New York¹⁴. Photochemical activity of different VOCs is closely associated with their molecular structures. Highly reactive VOC species such as isoprene and m-xylene exhibit $\bullet OH$ reaction rate constants (k_{OH}) up to the order of $10^{-11} \text{ cm}^3 \text{ molecule}^{-1} \text{ s}^{-1}$, resulting in a half-life as short as several hours^{15,16}. These compounds react with $\bullet OH$ and NO_x under sunlight irradiation, significantly promoting the generation of O_3 . Similarly, oxygenated VOCs (OVOCs) strongly contribute to atmospheric radical generation and O_3 formation due to their high photochemical reactivity¹⁷. In contrast, alkanes and halogenated hydrocarbons display lower reactivity compared to alkenes, with k_{OH} typically below $10^{-12} \text{ cm}^3 \text{ molecule}^{-1} \text{ s}^{-1}$. There are significant differences in the composition of VOCs released from various sources, and the proportions of alkenes, OVOCs, alkanes, and aromatics directly influence the potential for O_3 formation^{18,19}. Therefore, as O_3 pollution becomes increasingly severe, studying the interference effects of source apportionment on photochemical loss of VOCs (PL-VOCs) and their role in O_3 formation is highly valuable.

This study systematically investigates atmospheric VOC pollution in the PRD urban agglomeration, quantifying the concentrations and photochemical loss rates of 96 VOC species, evaluating the impacts of meteorological variations on PL-VOCs. To address the current challenges of ineffectively coordinating control of regional O_3 and VOCs, we developed a novel photochemical ozone formation potential (PL-OFP)-oriented source apportionment method to assess the source emission characteristics and health-economic burdens resulting from O_3 formation via photochemical transformation of VOCs (Fig. 1). Specifically, this study aims to address the

following questions: (a) Which VOC species or sources contribute most significantly to local O_3 formation? (b) What is the health-related economic burden associated with O_3 formation through the photochemical transformation of VOCs?

Results

Characteristics of VOCs in the PRD urban agglomeration

This study investigates the pollution characteristics of 96 VOC species in the atmospheric environment of four cities within the PRD region. These compounds were categorized into seven categories based on their characteristic functional groups, including alkanes, alkenes, alkynes, sulfides, aromatics, halogenated, and oxygenated VOCs (OVOCs). During the entire observation period, the mean concentration and standard deviation (SD) of TVOCs were 43.4 ± 23.0 ppbv (Fig. 2 and Table S1). Alkanes exhibited the highest concentration (21.7 ± 13.8 ppbv), accounting for 49.9% of total VOCs (TVOCs). Propane (6.98 ppbv), n-butane (3.79 ppbv), and isobutane (3.04 ppbv) were major contributors. Previous studies have indicated that alkanes such as n-butane and isobutane primarily come from natural gas emissions²⁰. Meng et al. also found that alkanes accounted for the highest proportion in the PRD region, reaching 55%²¹. In the PRD region, extensive natural gas pipeline networks have been built in residential areas, with coverage rates exceeding 80% in Guangzhou (GZ) and 93% in Shenzhen (SZ). Halogenated hydrocarbons (7.7 ± 3.39 ppbv) and aromatics (6.69 ± 6.12 ppbv) constituted the second and third most abundant VOC groups, accounting for 17.7% and 15.4% of TVOCs, respectively. Dichloromethane (4.15 ppbv) and toluene (3.88 ppbv) exhibited relatively high concentrations and proportions.

VOC concentrations exhibited significant spatial variations among the four cities ($p < 0.05$). The mean concentration of TVOCs was 29.4 ± 10.5 , 65.9 ± 28.3 , 31.9 ± 12.9 , and 43.4 ± 23.0 ppbv in GZ, Dongguan (DG), SZ, and Huizhou (HZ), respectively. DG, a typical industrial city, exhibited TVOC concentrations 1.2- to 2.2-fold higher than those in the other cities. Additionally, benzene series compounds in DG were 3.9- and 4.2-fold

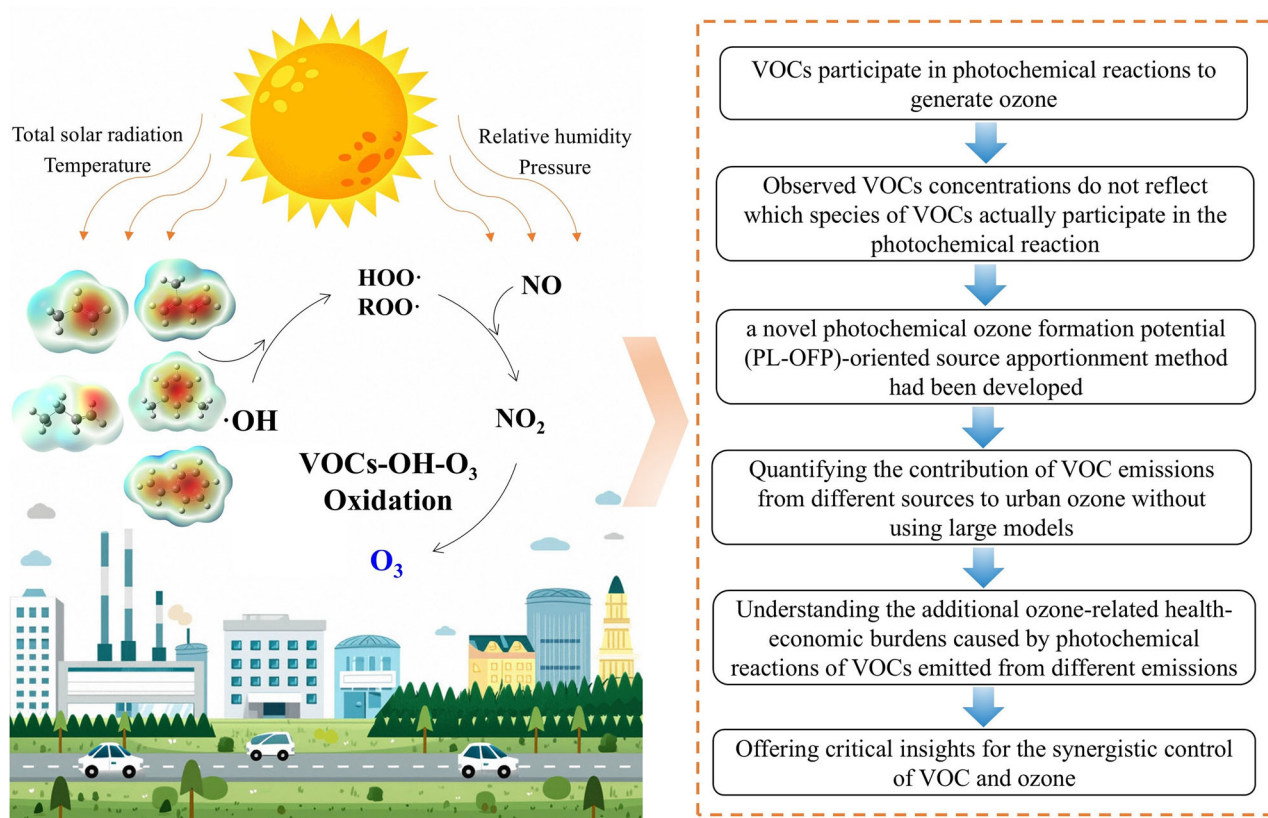


Fig. 1 | Photochemical reaction mechanisms of VOCs in the atmosphere: research ideas and objectives in this study.

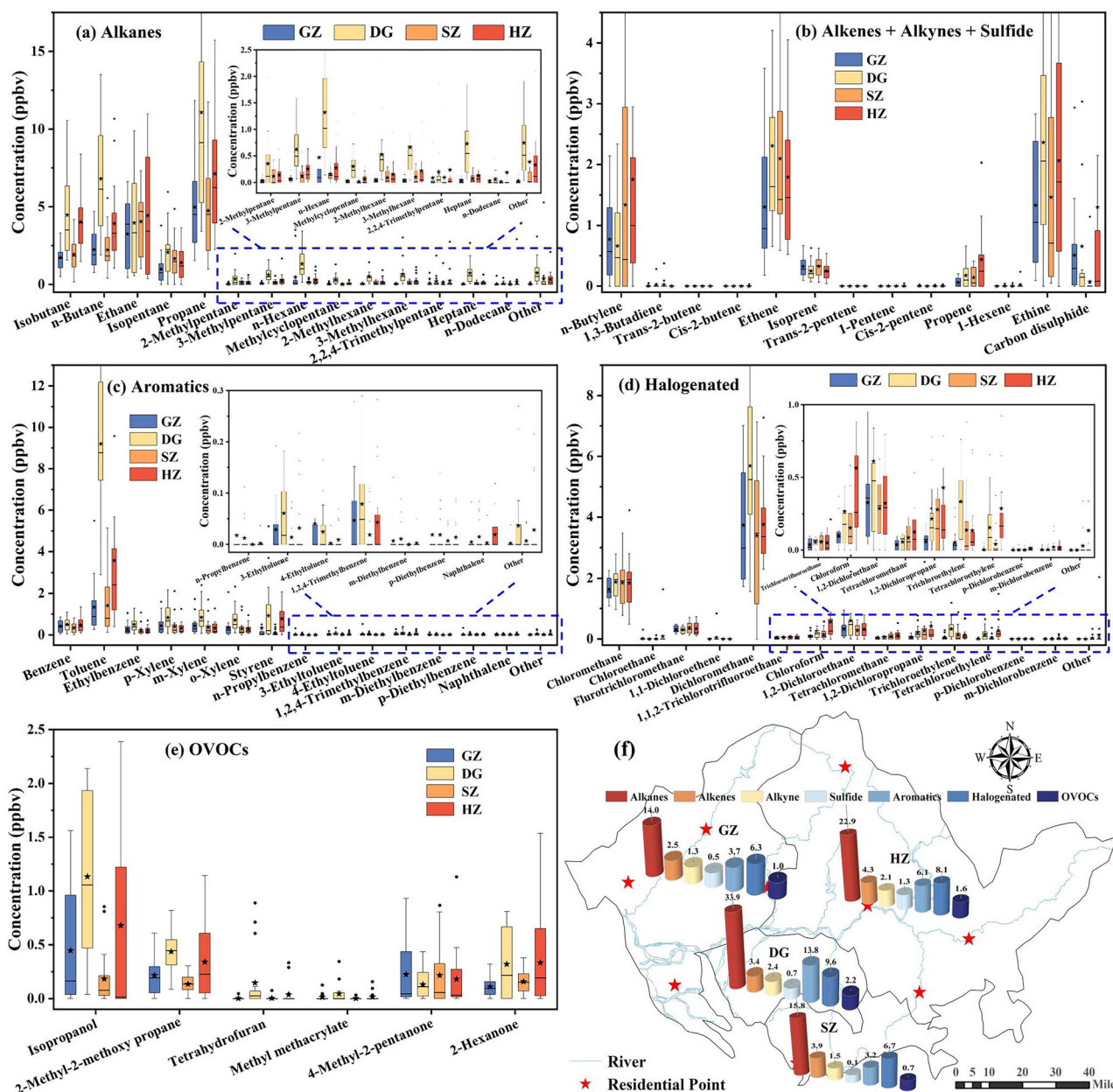


Fig. 2 | Concentration characteristics of VOCs in the PRD urban agglomeration. a–e Concentration profiles of the main compounds of different types of VOCs in GZ, DG, SZ, and HZ. **f** Regional concentrations of VOCs across the PRD urban agglomeration.

higher than in GZ and SZ, respectively, highlighting the substantial impact of industrial emissions on regional air quality²². Further analysis revealed that the gross output value (GDP) of secondary industry to local GDP in GZ, DG, SZ, and HZ were 25.3%, 55.4%, 37.8%, and 52.0%, respectively, which was consistent with the ranking of TVOC concentrations (DG > HZ > SZ > GZ). This suggests that cities with larger secondary industry proportions (such as electronic equipment manufacturing, chemical industry, etc.) exhibited greater VOC emissions and heightened potential for secondary pollution^{23,24}. Notably, halogenated hydrocarbons (HHs) in GZ and SZ accounted for 21.5% and 21.1%, respectively, significantly higher than DG and HZ. This difference can be attributed to more developed high-tech and related manufacturing industries, where the environmental concentrations of HHs were higher than those of low-industrialized areas²⁵. The economic focus and industrial structure of the city have a significant impact on the atmospheric VOC pollution profiles.

Seasonal VOC variations were significant in the PRD urban agglomeration ($p < 0.05$). The diurnal mean TVOC concentration was

36.4 ± 17.7 ppbv in summer and 50.3 ± 25.7 ppbv in winter (Fig. S1), with winter concentrations being 38.2% higher than those in summer. All cities consistently showed a trend of high in winter and low in summer, attributed primarily to lower temperatures in winter, facilitating surface cooling and formation of a stable inversion layer, limiting vertical air convection and pollutant dispersion²⁶. Additionally, increased rainfall in summer promoted VOCs removal via wet deposition²⁷. Conversely, isoprene and OVOCs displayed the opposite seasonal trend to TVOCs. Isoprene, a biological emissions marker^{28,29}, was higher in summer (GZ: 0.42 ± 0.18 , DG: 0.32 ± 0.18 , SZ: 0.41 ± 0.15 , HZ: 0.31 ± 0.16 ppbv), reflecting greater vegetation activity during the warmer season. Similarly, OVOCs, considered as secondary atmospheric products sensitive to temperature and solar radiation¹⁷, exhibited elevated OVOC concentrations in summer.

To better illustrate transport pathways and potential pollutant source regions in the PRD region, historical trajectories of air masses during summer and winter were analyzed using backward trajectory analysis. Figure S2 presents the results of 48-hour backward trajectory clustering at an

altitude of 500 m above ground level for both seasons. In summer, 89.1% of the air mass originated from the ocean, primarily driven by the thermal difference between land and ocean, with the air pressure gradient pushing the moist oceanic air masses inland³⁰. The prevailing southeast monsoon transports clean ocean airflow, diluting urban VOC concentration. The largest air mass cluster (30.8%) passed through Hong Kong, suggesting that emissions from Hong Kong influenced GZ, SZ, and nearby areas. In contrast, air mass movement patterns in winter were predominantly the opposite of those in summer. During winter, the PRD region was largely influenced by air masses originating from inland cities. Furthermore, due to significantly higher atmospheric pressure in winter, the region experienced stable atmospheric conditions²⁶ (Fig. 4), and the transport distances were shorter compared to summer, characterized by a dominance of mid-range transport. Two primary air mass clusters originated from northern cold air masses migrating southward from Jiangxi Province into the PRD region (accounting for 42.0% and 18.4%). Anthropogenic sources in Jiangxi, such as vehicular exhaust and combustion sources, emit substantial amounts of alkanes into the atmosphere³¹. These air masses increase local VOC concentrations in combination with PRD emissions through atmospheric migration.

Photochemical loss of VOC species

When analyzing the characteristics of atmospheric VOCs, directly observed concentrations can underestimate actual emissions due to the effects of photochemical reactions, particularly those involving •OH radicals^{13,15}. Figure 3 and Figure S3 present the photochemical loss diurnal data for the four cities in both summer and winter. The PL-TVOCs in summer were 3.9, 4.8, 3.8, and 3.2 ppbv for GZ, DG, SZ, and HZ, respectively. DG exhibited the highest photochemical loss, with aromatics contributing the most significantly (up to 2.2 ppbv), which were 6.2- and 5.5-fold higher than those of GZ and SZ, respectively. Styrene and toluene were the dominant contributors in PL-aromatics. Previous studies indicate that petroleum refining can emit substantial amounts of styrene¹⁴, while aromatic hydrocarbons such as toluene and ethylbenzene are widely used in industrial cleaning solvents, printing, and papermaking processes². The photochemical loss observed in DG suggests that some VOCs emitted from industrial activities are actively involved in local photochemical reactions. To account for uncertainties, Monte Carlo simulations were used to estimate annual PL-TVOCs in the PRD urban agglomeration (Fig. S4). The median PL-TVOCs was 1.72 ppbv, with a 95% confidence interval of 0.26–42.03 ppbv, which was slightly lower than the direct annual mean concentration. Sensitivity analysis indicated that isoprene was the dominant contributor, accounting for 44.2% of the annual PL-TVOCs.

The ratio of photochemical loss/initial concentration (P/I ratio) can better reflect the photochemical loss rate of VOCs (Table S2). Overall, alkenes exhibited the most significant photochemical loss, with P/I ratios of 59.2%, 38.0%, 35.1%, and 21.5% in GZ, DG, SZ, and HZ, respectively. Aromatic compounds followed as the second prominent contributors, with P/I ratios of 10.6%, 15.3%, 20.3%, and 17.3%. In contrast, alkanes (<3%) and alkynes (<1.5%) displayed relatively low photochemical loss rates due to their relatively stable chemical molecular structure. He et al. also observed alkanes and aromatics as the primary species contributing to local photochemical reactions in GZ during spring⁴. Although alkanes and HHs exhibited the highest detection frequency and concentrations among initial VOCs (In-VOCs), their contributions to the total-PL were below 3% and 1% across all four cities, respectively. Photochemical loss contribution is dependent on the molecular structure of compounds, with alkenes playing a particularly pivotal role. Alkenes, featuring unsaturated carbon-carbon double bonds (C=C), have π -bond electron clouds that are highly susceptible to be attacked by electrophilic groups or free radicals, leading to rapid photochemical consumption^{16,32}, such as isoprene (>65%) and butadiene (>44%).

The VOCs photochemical loss differed between winter and summer ($p < 0.05$). As displayed in Fig. 3 and S3, the PL-TVOCs in winter ranged from 0.7 to 2.0 ppbv, with DG exhibiting the highest loss. This range was approximately 19.2 to 57.5% lower than that of summer (3.2–4.8 ppbv), indicating weaker overall photochemical activity in winter. This

phenomenon can be primarily ascribed to shorter daylight hours and lower UV radiation intensity in winter, which slows the generation rate of •OH radicals and subsequent photochemical oxidation kinetics³³. He et al. also observed higher photochemical loss in summer compared to other seasons⁴. Isoprene exhibited the highest photochemical loss in winter, ranging from 0.21 to 0.45 ppbv. Although isoprene displayed relatively low concentration, the high reaction rate facilitated rapid photochemical consumption.

Given the significant seasonal variations in observed VOCs (Ob-VOCs) photochemical loss and the crucial role of diurnal solar radiation in driving photochemical reactions, it is particularly important to study diurnal changes in VOC concentrations. The photochemical loss characteristics of VOCs in the morning, noon, and nighttime were investigated. Our findings showed that the concentrations of Ob-VOCs in both summer and winter in the morning ($C_{\text{Summer}} = 37.2$ ppbv; $C_{\text{Winter}} = 52.9$ ppbv) and nighttime ($C_{\text{Summer}} = 44.9$ ppbv; $C_{\text{Winter}} = 59.4$ ppbv) were higher than those at noon ($C_{\text{Summer}} = 27.2$ ppbv; $C_{\text{Winter}} = 42.9$ ppbv), aligning with peak traffic hours. A comparison of different cities revealed that the daily variation difference between GZ and SZ was pronounced, likely due to the more concentrated spatiotemporal distribution of population movement and traffic emissions in these more developed cities. Human activities and traffic flow significantly influence atmospheric VOC levels^{18,19}. Notably, PL-VOCs exhibited an opposite diurnal trend, with significantly higher photochemical loss amounts at noon than in the morning and nighttime ($p < 0.05$), primarily driven by alkenes and aromatics. The key factor influencing atmospheric VOCs photochemical losses is not the concentration level, but rather the reactivity of VOC species with •OH radicals.

Meteorological variables associated with photochemical losses of VOC and O₃

Figures 4a, b show the seasonal and diurnal variations of meteorological factors in the PRD region. During summer, total solar radiation (TSR) exhibited a pronounced unimodal pattern, with the average daytime (6:00–18:00) radiation reaching 408.1 W/m², and midday peaks exceeding 800 W/m². This intense solar radiation, coupled with high temperatures ($T_{\text{noon}} = 32.0$ °C), creates a highly photochemically active environment³⁴. Atmospheric relative humidity (RH) and pressure displayed opposing trends, with RH exhibiting significant negative correlations with TSR ($r = -0.77$; $p < 0.05$) and temperature ($r = -0.96$; $p < 0.05$) (Fig. 4g), resulting in a low-humidity period lasting over four hours during the afternoon. While the diurnal patterns were generally consistent across seasons, atmospheric pressure was significantly higher in winter ($p < 0.05$). Under high-pressure weather conditions, the subsidence of air masses inhibited vertical diffusion, and horizontal wind speed decreased, facilitating the accumulation of pollutants in the ground layer¹⁶.

Meteorological factors significantly influence the photochemical losses of VOCs. Figure S5 shows the linear relationship between various meteorological factors and the ratio of photochemical loss of VOCs/observed VOCs (PL/Ob-VOCs). Our findings indicate that the PL/Ob-VOCs ratio is significantly higher in summer than in winter, indicating stronger photochemical activity of VOCs in summer. Further analysis of meteorological factors revealed that TSR significantly promoted the photochemical consumption of VOCs ($p < 0.05$), with greater sensitivity observed in summer (slope $k = 3.6 \times 10^{-3}$) compared to winter ($k = 1.2 \times 10^{-3}$). The PL/Ob-VOCs ratio increased more substantially with rising TSR in summer, suggesting that solar radiation plays an important role in the photochemical reactions³⁴. Furthermore, temperature exhibited a significant positive correlation with PL/Ob-VOCs in summer ($r^2 = 0.66$; $p < 0.05$), demonstrating that the photochemical reaction rate in summer was significantly higher than that in winter. At higher temperatures, VOC molecules acquire more kinetic energy, leading to increased effective collision frequencies and accelerated reaction rates³⁵. Berg et al. reported significant temperature-dependent reactivity of alkenes, aromatics, and alkanes with •OH, particularly between 280 and 340 K³⁶.

RH exhibited a negative correlation with PL/Ob-VOCs in both seasons. Specifically, VOC photochemical reactivity showed a significant negative correlation with RH ($r^2 = 0.64$; $p < 0.05$) when RH exceeded 75%.

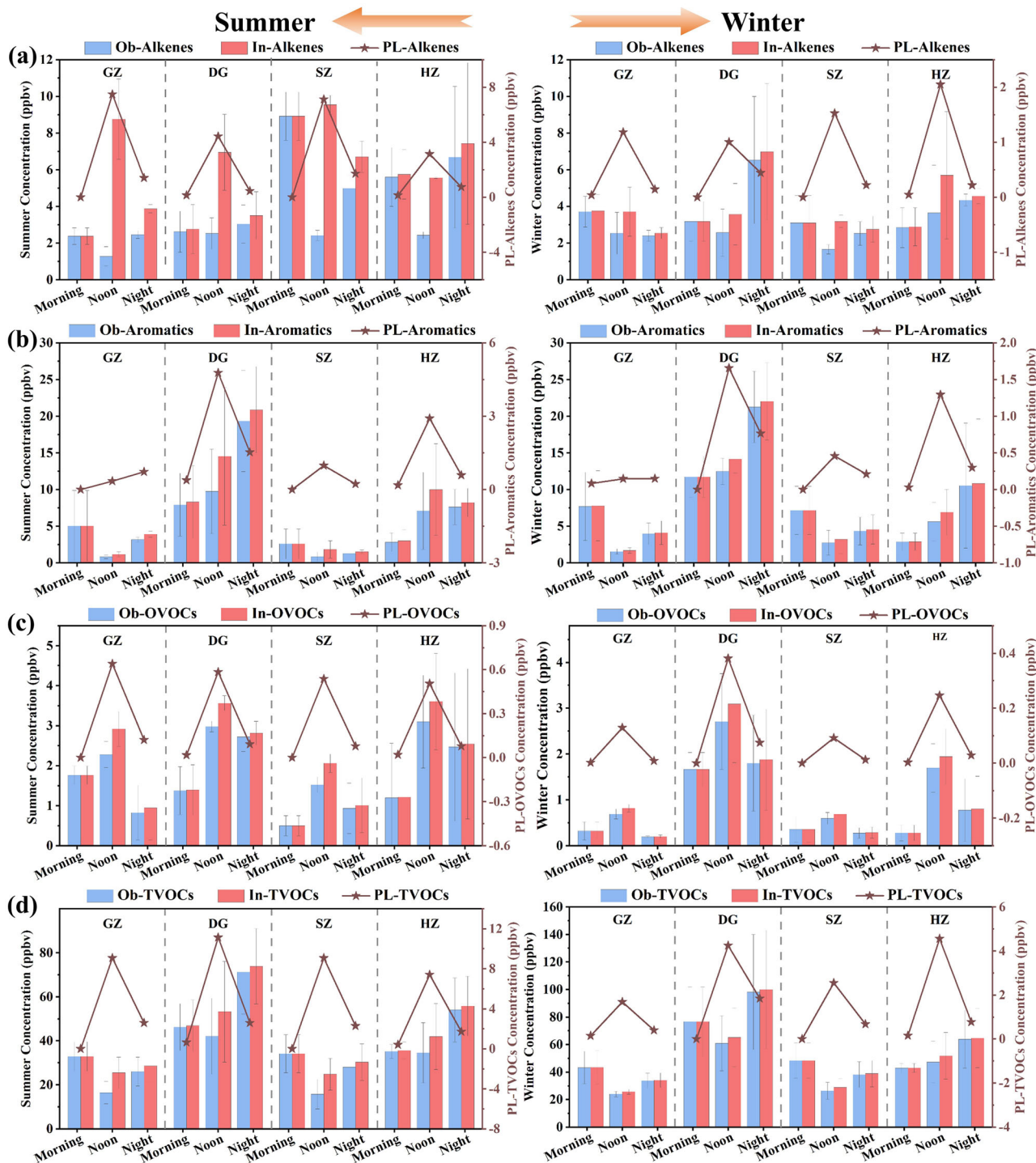


Fig. 3 | Spatiotemporal variations of observed, initial, and photochemical loss of VOCs. Concentrations of alkanes (a), aromatics (b), OVOCs (c), and TVOCs (d) (observed, initial, and photochemical loss) during summer and winter in the morning, noon, and night in the PRD urban agglomeration.

This effect may be attributed to the absorption of UV radiation by water vapor, decreasing near-ground light intensity³⁷. Furthermore, high relative humidity conditions reduce nitrous acid (HNO₂) concentration under polluted environments, with photolysis of HNO₂ being an important source of •OH production³⁸, thereby reducing atmospheric photo-oxidation capacity. Atmospheric pressure displayed a negative correlation with PL/Ob-VOCs in winter ($k = -0.33; p < 0.05$), indicating that higher pressure was associated with a reduced photochemical loss rate in winter. Although atmospheric pressure can promote secondary reactions of VOCs, its influence on the accumulation of VOCs appears to be relatively minor.

Seasonal comparisons revealed varying impacts of meteorological factors on PL/Ob-VOCs, with temperature and pressure exhibiting opposite trends across the two seasons. The photochemical reactions of VOCs in the atmosphere are influenced by the combined effects of multiple factors^{16,34,38}.

The characteristics of air quality parameter variations within the PRD region were discussed, as shown in Fig. 4c, d. The summer and winter data revealed a bimodal pattern for PM_{2.5}, with higher concentrations and poorer air quality observed during morning and night rush hours. Urban population mobility has an important impact on the urban air environment³⁹. The O₃ concentration exhibited a distinct unimodal pattern, with peak values

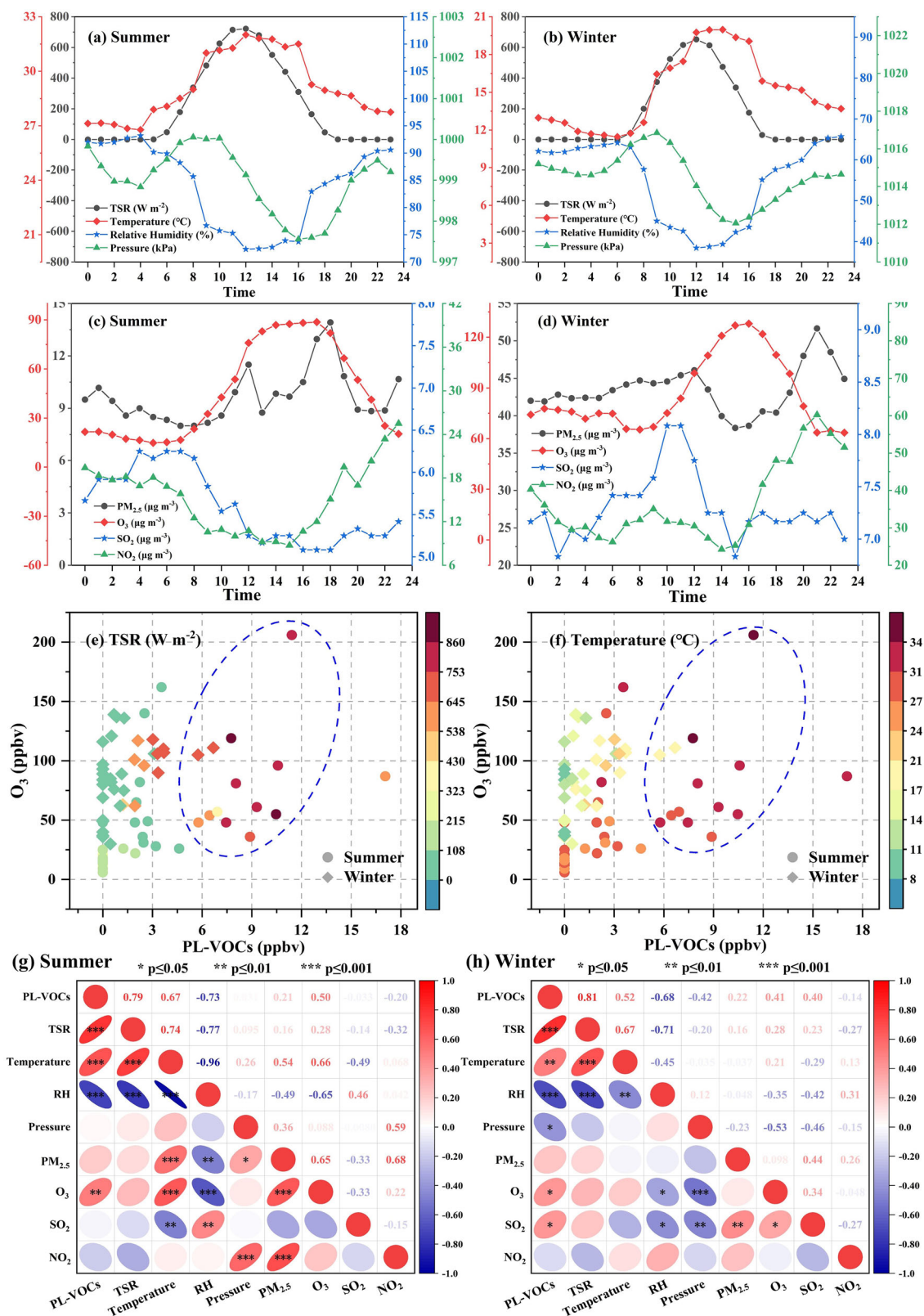


Fig. 4 | Meteorological factors and their relationship with photochemical loss of VOCs. Diurnal variation characteristics of meteorological factors in summer (a) and winter (b), diurnal variation characteristics of air quality parameters in summer (c) and winter (d), plot between O_3 and photochemical loss of TVOCs

(PL-TVOCs) with corresponding total solar radiation (TSR, $W m^{-2}$) (e) and temperature ($^{\circ}C$) (f) in all time, the pearson's correlation analysis between PL-TVOCs and meteorological parameters in summer (g) and winter (h) in the PRD urban agglomeration.

occurring at noon (reaching $88.7 \mu\text{g}/\text{m}^3$). A comparison with TSR revealed that the peak O_3 values lagged behind the solar radiation peak by 1–2 hours, a phenomenon observed in both winter and summer. This phenomenon is likely attributable to the maximum photochemical losses of VOCs occurring around noon. The rapid reaction of VOCs with hydroxyl radicals generates peroxy radicals, such as $\bullet\text{RO}_2$ and $\bullet\text{HO}_2$, which subsequently oxidize NO to NO_2 . Under photochemical conditions, NO_2 decomposes NO and O_3 ^{2,12}. The chain reaction of VOCs oxidation involves a time lag. The NO_2 concentration began to increase after 16:00, coinciding with a decrease in O_3 concentrations. This can be attributed to the primary source of NO_2 emissions coming from traffic⁴⁰, with the evening rush hour leading to increased NO_2 levels. Furthermore, the gradual accumulation of NO generated by photolysis, coupled with weakening the TSR, which strengthens the reaction of $\text{O}_3 + \text{NO} \rightarrow \text{NO}_2 + \text{O}_2$ ⁴¹, the formation of NO_2 consumes part of the atmospheric O_3 . The formation and consumption of O_3 are inextricably linked to VOCs and NO_x . Therefore, effective O_3 control strategies in urban areas should prioritize the synergistic reduction of VOCs and NO_x emissions.

VOCs serve as crucial precursors for O_3 formation. To further elucidate the influence of meteorological factor variations on photochemical loss of VOCs and O_3 formation, this study provides a visual representation of the relationships between meteorological factors and both PL-VOCs and O_3 , as shown in Fig. 4 and S6. The study revealed that elevated levels of TSR and temperature (red markers) were associated with increased concentrations of both PL-VOCs and O_3 . Conversely, when RH exceeded 75%, the concentrations of both PL-VOCs and O_3 decreased. TSR, temperature, and RH primarily affect O_3 formation by influencing the atmospheric reactions of VOCs³, thereby simultaneously affecting the variations in PL-VOCs and O_3 concentrations. Under higher atmospheric pressure (red markers), lower PL-VOCs but elevated O_3 concentrations were observed. This phenomenon may be attributed to the formation of an inversion layer caused by the subsidence of air masses under higher pressure conditions, which promotes O_3 accumulation in the ground layer¹⁶. However, the effect of pressure on photochemical loss is relatively limited, resulting in asynchronous variations between PL-VOCs and O_3 . Atmospheric pressure primarily influences pollutant concentration by affecting atmospheric dispersion through physical processes.

Potential contributions of VOCs to O_3

Depending on their characteristic functional groups and molecular structures, different VOC species form O_3 at distinct rates and through different mechanisms. This study aimed to comprehensively evaluate the impact of local VOCs emissions on O_3 formation by calculating the ozone formation potential (OFP) in the PRD urban agglomeration. Our findings revealed that the OFP concentrations for photochemical loss of VOCs (PL-OFP) were positively correlated with daily maximum 8-hour average ozone (DMA8-O_3), notable in summer ($r^2 = 0.48$; $p < 0.05$), as shown in Fig. S7. Investigating the contributions of various VOC categories to O_3 formation (Fig. 5 and Fig. S8), we found that alkenes contributed the most to the PL-OFP, accounting for 66.0%–93.1% in summer and 45.7%–77.8% in winter, respectively. Monte Carlo simulations revealed an annual PL-OFP of 10.46 ppbv, with a 95% confidence interval of 0 to 104.57 ppbv (Fig. S9). In summer, with stronger sunlight irradiation, the contribution of alkenes to O_3 formation was 4.0 times greater than that in winter. This $h\nu$ is because the relatively low steric hindrance of C=C bonds, which facilitates their participation in the reaction of $\text{NO}_x + \text{VOCs} + \text{OH} \rightarrow \text{O}_3 + \text{secondary pollutants}$. The rapid reaction of VOCs with hydroxyl radicals generates peroxy radicals, such as $\bullet\text{RO}_2$ and $\bullet\text{HO}_2$, which subsequently oxidize NO to NO_2 . Under photochemical conditions, NO_2 then decomposes to form NO and O_3 ^{2,12}. Isoprene, primarily emitted from biological sources^{28,29}, is a significant contributor to PL-OFP, accounting for 56.3% in summer and 37.3% in winter, with an annual sensitivity to PL-OFP reaching 49.0%, highlighting the substantial role of biological VOCs in O_3 formation in South China.

Aromatics also made significant contributions to OFP, accounting for 13.2% in summer and 26.1% in winter. Particularly in DG, the city with the highest proportion of secondary industry among the four cities, the contribution of aromatics to OFP reached 28.5% in summer and 42.6% in

winter. The major aromatic contributors were toluene, m-xylene, and styrene, which are primarily derived from anthropogenic sources^{13,42}. Sensitivity analysis for Ob-OFP and In-OFP showed that toluene had the highest sensitivity among aromatics, reaching 33.8% and 37.0%, respectively. These findings highlight the significant influence of anthropogenic sources on the local atmospheric environment, with detailed VOCs source apportionment provided in Fig. 6. Although alkanes had the highest detection rate and concentration, their contribution to PL-OFP accounted for only 0.7%–2.9% in summer and 1.4%–5.7% in winter, which was much lower than that of alkenes and aromatics to O_3 formation. Based on the above analysis, it can be concluded that the primary factor influencing O_3 formation is the reactivity of VOC compounds rather than their actual atmospheric concentrations.

The contribution of photochemically reactive VOCs to O_3 formation varied across cities and seasons, as illustrated in Fig. S8. SZ exhibited the highest contribution rate in summer, reaching $52.9 \pm 24.7\%$, with isoprene (27.2%) being the primary contributing compound. In contrast, HZ and DG showed the highest contribution rates in winter, reaching $8.8 \pm 3.0\%$ and $8.8 \pm 2.7\%$, respectively, with distinct key contributing species. In HZ, isoprene (2.9%) and n-butene (2.1%) were the dominant contributors, while in DG, the contribution of isoprene decreased to 1.9%, and the industrial source compounds, such as ethylene (1.3%), toluene (1.5%), and m-xylene (1.0%), showed a significant increase. These variations indicate that the city-specific industrial structure significantly influences the characteristics of atmospheric VOCs and their contribution to O_3 formation^{23,24}. Furthermore, the VOC photochemical conversion contribution rates were generally higher in summer (20.1%–69.1%) than in winter (4.2%–12.2%). High temperatures and intense light intensity in summer significantly enhance VOC photolysis rates and increase the concentration of free radicals³⁴, resulting in a 3.7- to 9.8-fold increase in the contribution rate of O_3 formation compared to winter. Overall, this study demonstrated that spatial variations in O_3 contributions induced by VOCs within the PRD urban agglomeration are closely related to the characteristics of VOC emission sources, while seasonal variations are dominantly driven by meteorological factors.

PL-OFP-oriented source apportionment

The Positive Matrix Factorization (PMF) model was employed to quantify the emission sources of VOCs in the PRD urban agglomeration. Based on a comparison of the Q_T/Q_R ratios derived from the PMF model (Fig. S10), six potential emission source factors were ultimately selected in both summer and winter⁴³. The specific source profiles are presented in Figs. S12 and S13, while the detailed contribution of VOC compounds to the six emission sources is provided in Text S8.

Figures 6c, d show the proportion of potential VOC emission sources in the PRD urban agglomeration before and after photochemical reactions. Summer Ob-VOC data revealed that natural gas and biomass combustion (NGBC) contributed the most (26.0%), followed by vehicle emissions (19.1%) and biogenic sources (15.3%). In winter, NGBC (25.0%), polymer production-related industrial source (PPIS) (20.7%), and vehicle emissions (20.6%) were the major contributors. NGBC was the largest emission source in both summer and winter. This is primarily due to the widespread use of safer and lower-carbon natural gas in the PRD region, with over 80% and 93% coverage in GZ and SZ. Furthermore, the population density and vegetation coverage in the PRD urban agglomeration are high, aligning with the background survey. Notably, the observed and initial contributions of PPIS in winter were significantly higher than those in summer ($\Delta \sim 6.8\%$). This is likely because the short-chain alkanes emitted from this source are more prone to accumulation under low reaction activity and limited air mass migration conditions^{3,16}. The contribution from biological emissions (BE) was significantly higher in summer than in winter ($\Delta 6.9\%$), primarily due to increased plant activity.

Based on the VOC emission source apportionment results, further combination with ozone formation potential revealed the actual contribution intensity of each pollutant source to O_3 formation, as shown in Figs. S15 and S16. Due to varying species reaction activity, the proportions of the six emission sources based on OFP differed from their observed values. Vehicle emissions (VE) (22.7%) and NGBC (17.7%)

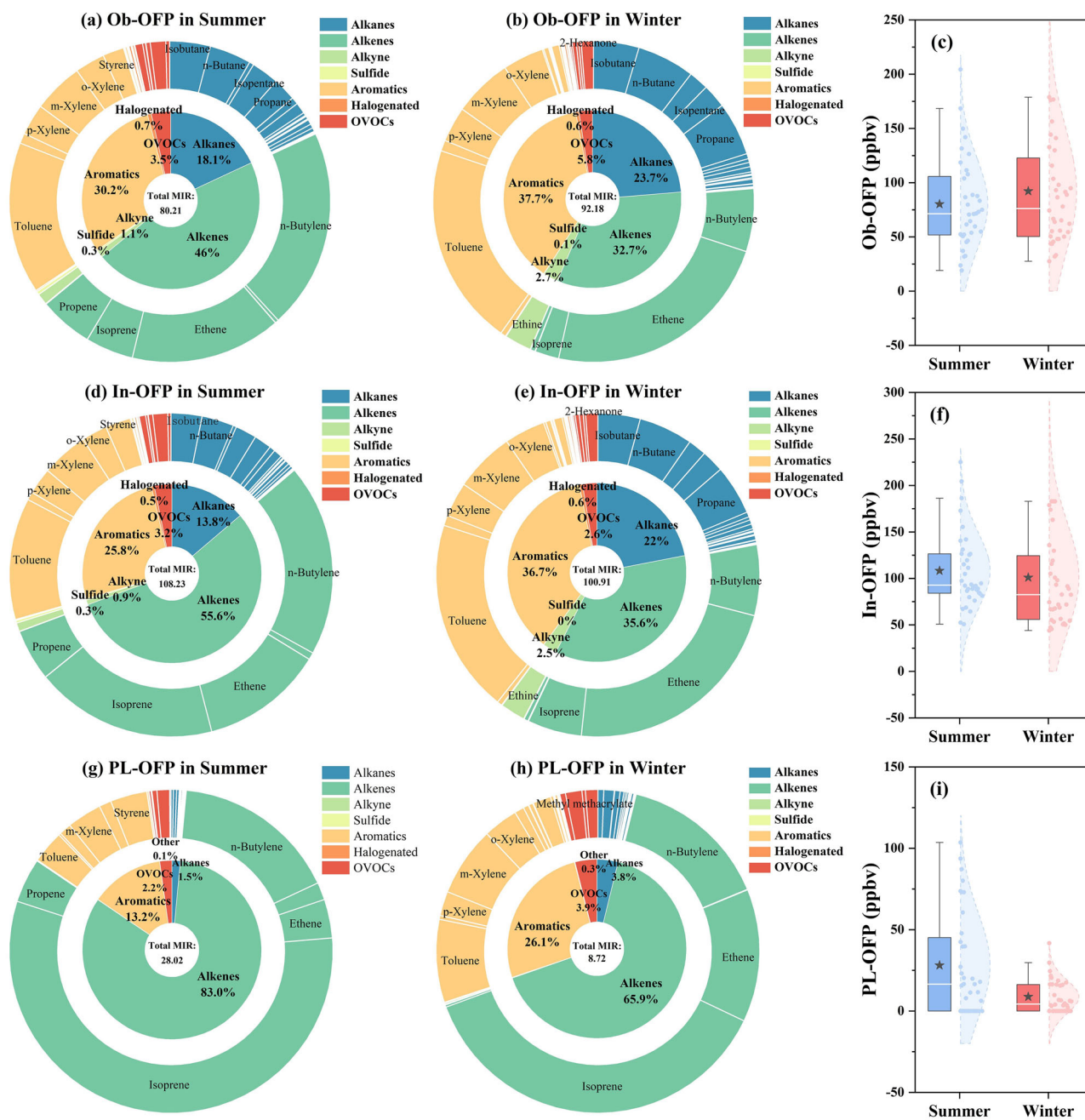


Fig. 5 | Ozone formation potential based on observed, initial, and photochemical loss of VOCs. The proportion of Ob-OFP in summer (a), Ob-OFP in winter (b), In-OFP in summer (d), In-OFP in winter (e), PL-OFP in summer (g), PL-OFP in

winter (h) of VOC species with ozone formation potential, the concentration characteristics of Ob-OFP (c), In-OFP (f), PL-OFP (i) in summer and winter.

were the major contributors to OFP in summer, whereas vehicle emissions (24.2%) and PPIS (24.1%) dominated in winter, indicating that VE-VOC has the greatest potential for O₃ contribution throughout the year. The enhanced OFP of industrial sources in winter may be related to the accumulation of surface VOCs and adjustments in production activities⁴⁴. Comparing the initial and observed OFP proportions revealed a significant consumption effect of highly reactive VOC emission sources during photochemical reaction. The initial OFP percentage of biological emissions sources in summer (26.9%) decreased to 11.1% after photochemical conversion. Biogenic sources constituted the largest actual contributor to O₃ formation, accounting for 64.9% in summer. NGBC, as the second largest actual contributor, accounted for only 5.7% in summer but reached 46.7% in winter. In contrast, the initial OFP percentage of PPIS in winter (21.95%) increased to 24.13%

after photochemical reaction, suggesting that PPIS emitted VOCs may contain more medium- to low-reactivity components that gradually participate in O₃ formation over longer reaction times¹⁵. Notably, vehicle emissions exhibited the highest overall annual OFP; however, their actual contribution to O₃ formation accounted for merely 3.3% when considering photochemical loss. The conclusions derived from our PL-OFP-oriented source apportionment method significantly differ from those obtained through direct OFP calculations. Consequently, policy recommendations based solely on traditional source apportionment or OFP assessments are limited, posing challenges for the coordinated control of VOCs and O₃. These findings suggest that effective O₃ control strategies should take into account not only the intensity of VOC emission sources but also the reactivity of individual VOC species.

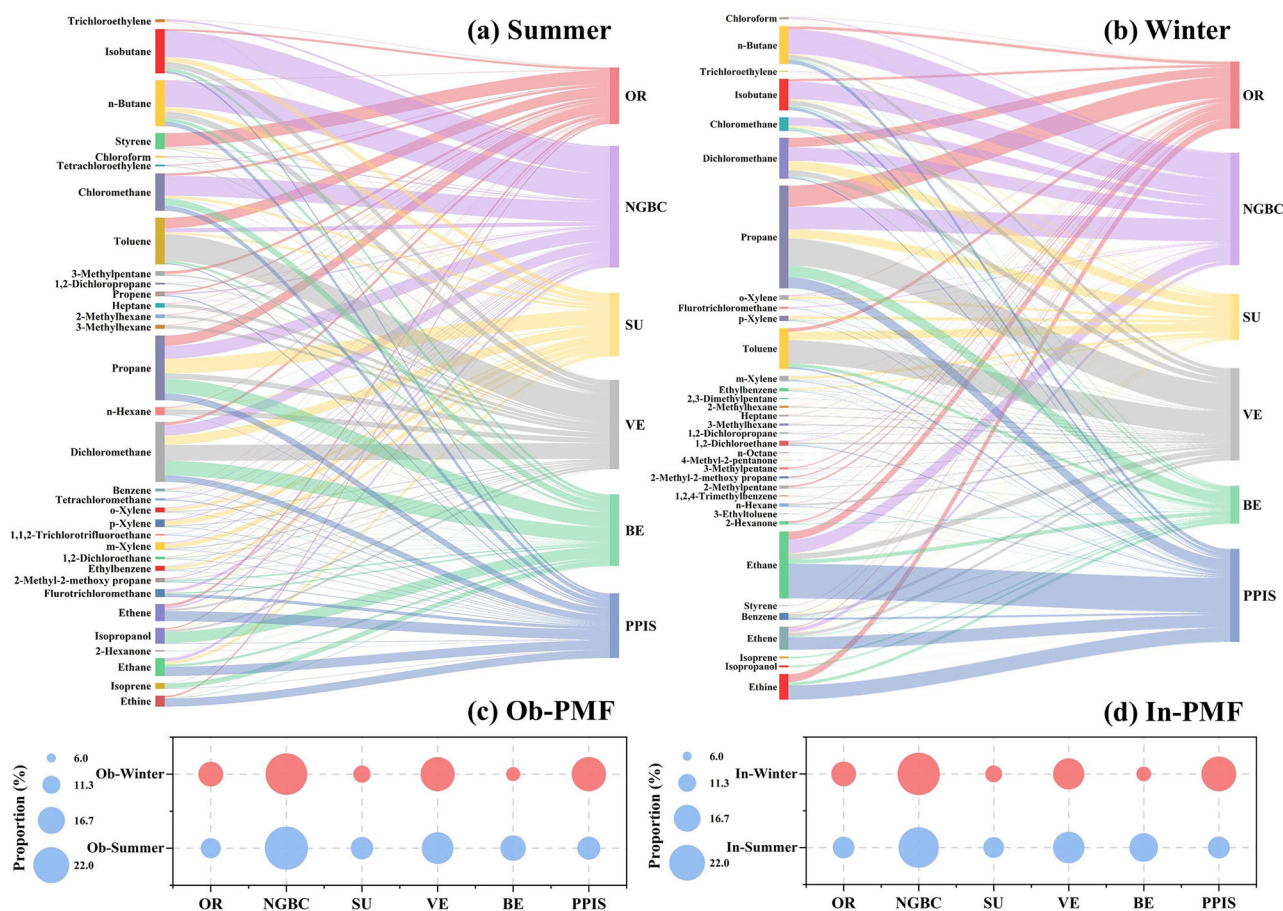


Fig. 6 | Source apportionment of VOCs using the PMF model. The contribution of Ob-VOCs compounds in the PRD urban agglomeration to six emission sources during summer (a) and winter (b) based on the PMF model, the proportion of six emission sources in Ob-PMF (c) and In-PMF (d).

O₃-related health-economic burdens

Exposure to O₃ increases the risk of cardiovascular and respiratory diseases among local residents. This study estimated the all-cause, respiratory, and cardiovascular non-accidental premature mortality rates attributable to short-term O₃ exposure in different cities. The results are shown in Fig. 7. A comparison across different cities reveals significant variation in the health effects of O₃ pollution. GZ, a core megacity and the provincial capital, exhibited medium-to-high values (red-brown) for all-cause and cardiovascular mortality rates across most of its area. Furthermore, the mortality rates for various diseases were generally higher in GZ compared to other cities. The number of O₃-related all-cause mortality in GZ (5708 cases) far exceeded those in DG (1,322 cases), SZ (821 cases), and HZ (671 cases), accounting for 3.0‰, 1.3‰, 0.5‰, and 1.1‰ of the total population in these cities, respectively. Despite SZ also being a megacity, the all-cause, respiratory, and cardiovascular non-accidental mortality rates in GZ were 7.0, 6.0, and 4.3 times higher than those in SZ, respectively. This is primarily because GZ has a longer history and a larger population. In terms of age structure, the population aged 60 and above accounted for 19.38% in GZ, which is 3.6 times that of SZ (<https://wsjkw.gd.gov.cn/>). With an aging demographic, the mortality rate in GZ (7.35%) was also significantly higher than in other cities. Urban population density and age structure significantly influence O₃-related health risks⁷. The O₃-related health risk presented a stepwise distribution: “all-cause > cardiovascular > respiratory”. O₃ mainly enters the human body through the respiratory tract, stimulating alveolar epithelial cells in the lungs, activating the nuclear factor-κB and antioxidant pathways. This leads to the overproduction of inflammatory mediators, such as IL-1 and IL-17⁴⁵. These inflammatory mediators enter the blood circulation and spread throughout the body, causing organ inflammation and vascular dysfunction. Additionally, O₃ can attack lipids on cell membranes, resulting in the production of

lipid peroxides, such as the intracellular peroxisomal fatty acid β-oxidase⁵ and 9-HpODE⁶, accelerating the process of atherosclerosis and leading to cardiovascular and respiratory diseases.

The health risks associated with O₃ formation from photochemical loss of VOCs were also quantified, as shown in Fig. S17. The results revealed that the four cities experienced up to 2055 cases of non-accidental premature mortality due to the PL-VOCs converted to O₃ formation. Among the cities, GZ experienced the highest health burden from PL-VOCs converted to O₃, with the all-cause, cardiovascular, and respiratory premature mortality reaching 1438, 456, and 190 cases, respectively. Additionally, PL-VOCs converted to O₃ in GZ contributed the most to the local O₃-related health risk, accounting for 25.2%, 25.2%, and 25.0%, respectively. Isoprene, n-butene, and m-xylene were the primary contributing compounds, with biological emission and NGBC making the most significant contributions. The O₃-related all-cause mortality caused by biological emission and NGBC reached 1162 and 273 cases (Fig. S18), respectively. Highly reactive VOC emission sources should be prioritized for control.

The health economic losses (HEL) resulting from O₃-related health risks were further quantified using the value of statistical life method⁴⁶. As shown in Fig. 7d and S19, we found that GZ, which suffered the highest O₃-related health risks, also experienced the greatest economic losses, with all-cause HEL reaching \$3475.9 M, accounting for 8.0‰ of the total GDP. DG, with the highest proportion of secondary industry, followed as the second largest contributor, with all-cause HEL reaching \$677.7 M. Although SZ had lower O₃-related mortality than HZ, its higher per capita disposable income and willingness to pay for health consumption resulted in a significantly higher all-cause HEL of \$488.8 M, which was 1.7 times that of HZ. Economic losses caused by PL-VOCs converted to O₃ were calculated, and the economic losses caused by all-cause mortality in GZ, DG, SZ, and HZ were \$875.7, \$140.5,

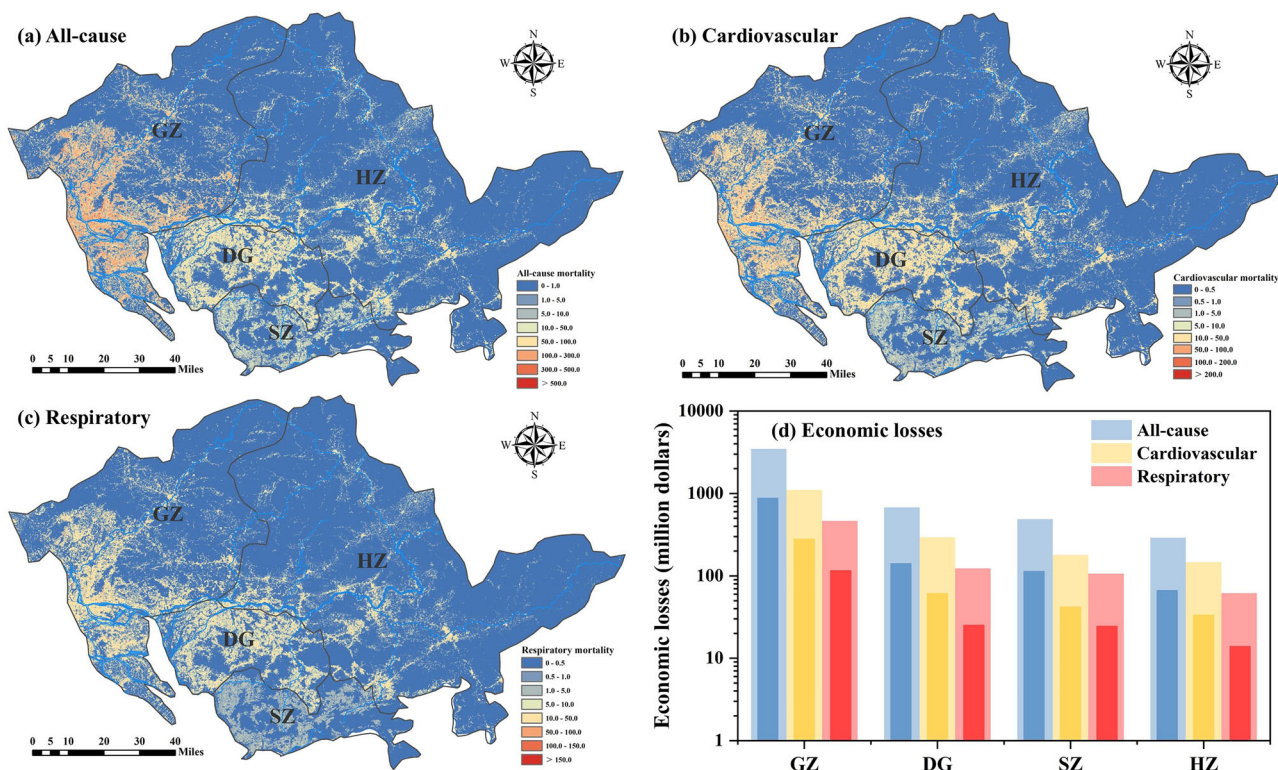


Fig. 7 | Health risks and economic losses attributed to ozone exposure. The spatial distribution of the mortality of all-cause (a), cardiovascular (b) and respiratory (c) due to O₃ short-term exposure in the PRD urban agglomeration (10² km²), the city-

specific economic losses (d) of O₃-related diseases (The outer bars represent the economic loss caused by O₃, while the inner bars represent the economic loss caused by the PL-VOCs converted to O₃).

\$113.1, and \$66.3 million, respectively, accounting for 2.0%, 0.82%, 0.22%, and 0.77% of the local urban GDP. To address uncertainty, Monte Carlo simulations were used to estimate the economic loss from PL-VOCs converted to O₃ across the PRD urban agglomeration (Fig. S20). The median value was \$1203.6 M, with a 95% confidence interval ranging from \$932.4 million to \$3173.9 million. Biogenic sources accounted for the dominant contributor, resulting in \$680.4 million in economic losses. The health risk associated with the PL-VOCs converted to O₃ cannot be overlooked in the PRD urban agglomeration. Notably, the proportion of HEL caused by different diseases was significantly varied between cities. In HZ, the HEL caused by cardiovascular disease reached 50.5%, which is 16.8% higher than in GZ (31.7%). In DG, the HEL caused by respiratory disease was the highest (21.8%). These variations reflect the complex interplay among urban functional positioning, environmental exposure characteristics, population structure, and resource distribution in different cities⁴⁷. Atmospheric VOCs not only pose direct carcinogenic risks to residents^{19,48}) but also contribute to the O₃ formation through photochemical reaction, leading to significant health effects and substantial economic losses in local cities.

Discussion

This study conducted photochemical loss calculations and model analyses for 96 VOC species in the PRD urban agglomeration during summer and winter. The results indicated that the annual average TVOC concentration in the PRD region was 43.4 ppbv, with alkanes and halogenated hydrocarbons being the dominant components. DG exhibited concentrations 1.2–2.2 times higher than other cities due to high secondary industry density. Alkenes (such as isoprene, butadiene) and aromatics (such as styrene) were the dominant reactive species under photochemical loss due to their high reactivity, consumed by reacting with •OH. Meteorological factors, particularly TSR and temperature, significantly promoted •RO₂ and •HO₂ formation from VOCs oxidation ($p < 0.05$), while RH had the opposite pattern. Atmospheric pressure primarily influences air mass transport. Assessment of O₃ formation potential revealed that alkenes exhibited the highest PL-OPF, followed by

aromatics. PMF analysis identified six emission sources, with NGBC as the largest source, and vehicle emissions exhibited the greatest potential for O₃ formation. Notably, after photochemical reaction, over 70% of biological sources were consumed, making it the dominant actual O₃ contributor. Consequently, greater emphasis should be placed on controlling low-concentration but highly reactive VOCs in the PRD. Quantification of O₃-related health-economic burdens revealed that GZ experienced the highest health risks (5708 cases), primarily from biological emissions and NGBC. The all-cause HEL in the PRD reached \$4999.4 M, accounting for 4.09% of the total GDP, of which the PL-VOCs contributed \$1195.6 M. This study elucidates the key mechanisms of photochemical loss of VOCs and their impact on O₃ formation and health-economic effects, providing a theoretical basis for the development of synergistic VOCs and O₃ control policy.

Methods

Site description

In this study, VOC samples were collected during summer from July 17th to August 4th, 2024, and in winter from December 20th, 2024, to January 7th, 2025, with diurnal sampling conducted at 7:00 am, 12:00 noon, and 7:00 pm. Sampling was conducted in four cities within the PRD urban agglomeration of China: Guangzhou (GZ), Dongguan (DG), Shenzhen (SZ), and Huizhou (HZ). GZ and SZ are megacities with a significant presence of high-technology industries. DG has a secondary industry proportion of 55.4%, with its electronics manufacturing sector exceeding one trillion RMB in scale. HZ hosts several large-scale state-owned petroleum refining enterprises, with an annual petrochemical production capacity of 42 million tons, and features substantial vegetation coverage reaching 61.6% (<https://www.gd.gov.cn/>). These cities exhibit distinct economic landscapes, industrial compositions, and population structures, making them ideal for studying city-specific VOC pollution characteristics. Figure S21 shows the land use types of a 10 m spatial grid in these cities. During the study period, the weather was predominantly sunny or cloudy, and meteorological data were obtained from the Guangdong Meteorological Bureau (<http://gd.cma.gov.cn/>).

Hourly meteorological factors, including total solar radiation ($W\ m^{-2}$), temperature ($^{\circ}C$), humidity (%), and atmospheric pressure (hPa), as well as air quality parameters, including $PM_{2.5}$, O_3 , NO_2 , and SO_2 , were recorded concurrently. All samples were collected using specially passivated 2.7-liter Summa canisters (ENTECH Instruments Inc., Silonite™). To better represent urban VOC pollution levels, all sampling sites were located on the rooftops of tall buildings, and the sampling port was set 1.5 m above the rooftop surface. Detailed sampling information is presented in Table S5.

Monitoring instruments

In accordance with optimized methodologies from the U.S. Environmental Protection Agency (EPA) and previous studies by our research group^{5,49}, 96 VOC species were analyzed through pre-concentration coupled with gas chromatography flame ionization detector/mass spectrometry (GC-FID/MS). A detailed methodological description is provided in Text S1 and Text S2. Briefly, VOCs were concentrated via a pre-concentration system and subsequently rapidly injected into GC-FID/MS. Using a split mode configuration, conventional VOCs were separated by a DB-1 column ($60\ m \times 0.25\ mm \times 1.0\ \mu m$, Agilent Technologies, U.S.) and detected by MS, while short-chain aliphatic hydrocarbons were separated using a retention gap and HP-AK/S-PT column ($30\ m \times 0.32\ mm$, Agilent Technologies, U.S.) and detected by FID. Photochemical assessment monitoring stations (PAMS) and TO-15 standard samples (Linde Spectra Environment Gases, USA) were analyzed. VOCs were quantified using an internal standard calibration method (1,4-difluorobenzene, chlorobenzene- d_5 , bromochloromethane, and 4-bromofluorobenzene). Sample dilution was performed with an Entech 4700 dynamic dilution system. Detailed information on the analyzed compounds is provided in Table S6.

Estimation of the photochemical loss of atmospheric VOCs

VOCs exhibit high photochemical reactivity under sunlight irradiation, and their photochemical loss assessment is commonly based on the variation of species' atmospheric reaction with $\bullet OH$. The initial concentration ratio of paired species (C/B) is primarily controlled by their common emission source, while the observed ratio ($\Delta C/B$) gradually decreases due to the differences in photochemical consumption rates during the atmospheric transport process. By integrating the real-time concentration ratio of C/B combined with a photochemical age (Δt) calculation model, the OH exposure ($[OH] \cdot \Delta t$) experienced by VOCs can be quantitatively estimated^{13,15}. The specific formulas are:

$$\Delta t = \frac{1}{(K_c - K_b)[OH]} \times \left[\ln \left\{ \frac{[C]}{[B]}, t = 0 \right\} - \ln \left\{ \frac{[C]}{[B]}, t = t \right\} \right] \quad (1)$$

$$[VOC_i]_{0,t} = [VOC_i]_t / \exp(-k_i[OH]\Delta t) \quad (2)$$

$$[VOC_i]_{loss,t} = [VOC_i]_{0,t} - [VOC_i]_t \quad (3)$$

Where B and C represent pairs of photochemical reaction species, two VOCs with a common source and different photochemical reaction rates. The rate constants K_b and K_c present the reaction rate with OH radicals for species B and C, respectively. In this study, Figure S22 illustrates the strong correlation ($R^2 = 0.98$; $p < 0.01$) between ethylbenzene (E) and m/p-xylene (X), indicating a strong linear regression relationship, and indicating that they mainly come from a common source. Previous studies have found that ethylbenzene and m/p-xylene are often emitted from industrial solvent usage⁵⁰. Furthermore, their various OH reaction rates ($k_E[OH] = 7.0 \times 10^{-12}\ cm^3\ molecule^{-1}\ s^{-1}$, $k_X[OH] = 18.7 \times 10^{-12}\ cm^3\ molecule^{-1}\ s^{-1}$) make them ideal photochemical reaction species pairs in this study^{51,52}. The reaction rate constants for each VOC with OH radicals ($K_i[OH]$) are presented in Table S7. $\left\{ \frac{[C]}{[B]}, t = 0 \right\}$ and $\left\{ \frac{[C]}{[B]}, t = t \right\}$ are described in Text S3.

Calculation of excess risks

The log-linear exposure-response model, widely applied in epidemiology and risk assessment, describes the potential relationship between pollutant exposure levels and health outcomes. In this study, this model was utilized to investigate the excess mortality risks due to O_3 exposure for all-cause, cardiovascular, and respiratory diseases^{7,53}. The formula for calculating excess risks is as follows:

$$ER_{i,city} = \begin{cases} 0 & \text{for } C_i < C_{i,0} \\ \exp \left[\beta_i (C_{i,city} - C_{i,0}) \right] - 1 & \text{for } C_i \geq C_{i,0} \end{cases} \quad (4)$$

$$H_{i,city} = BI_{i,city} \times EP_{city} \times ER_{i,city} \quad (5)$$

Where $H_{i,city}$ represents deaths attributable to disease i (all-cause, cardiovascular, and respiratory diseases) caused by O_3 exposure in the target cities; $BI_{i,city}$ represents the health baseline incidence of the corresponding disease i; EP_{city} refers to the city's population; $ER_{i,city}$ represents the excess risk of disease i caused by O_3 exposure in the target cities, calculated using Eq. (4); The exposure-response coefficient (β_i) for disease i are obtained from Chinese epidemiological studies, with detailed parameters provided in Table S7; $C_{i,city}$ is the daily maximum 8-hour average O_3 concentration (DMA8- O_3), and $C_{i,0}$ represents the threshold concentration. Since the relationship between ozone exposure and short-term mortality risk is approximately log-linear with no apparent threshold within common ambient concentration ranges⁵⁴, this study employs the theoretical minimum exposure level for calculation, and $C_{i,0}$ was set to zero in this study⁵⁵.

Estimation of economic loss

The Value of Statistical Life (VSL) is an economic concept commonly utilized in epidemiology to represent the public's willingness to pay for reductions in mortality risk⁴⁶. Since China does not provide a standardized VSL value for the four cities examined in this study, we employed the benefit transfer method, using per capita disposable income as an index to estimate the VSL for the target cities. The mathematical model is as follows:

$$VSL_{k,city} = VSL_{base} \times \left(G_{k,city}, I, G_{base} \right)^{\beta} \quad (6)$$

$$EL_{i,k,city} = VSL_{k,city} \times HI_{i,k,city} \quad (7)$$

Where $VSL_{k,city}$ represents the estimated VSL for the target city in year k; VSL_{base} is the VSL value for the target cities based on existing studies. We referenced the 2019 statistical data for Beijing estimated⁵⁶, with a value of \$55.23 M; β is the income elasticity, set to 0.8, as recommended by the OECD⁵⁷; and $EL_{i,k,city}$ represents the economic losses from O_3 -related diseases in year k for the target cities.

Data analysis

In this study, EPA PMF 5.0 was used to analyze the source apportionment for the PRD urban agglomeration during both summer and winter. The analysis aimed to investigate the contributions of each compound in observed VOCs (Ob-VOCs), initial VOCs (In-VOCs), and PL-VOCs to potential emission sources, and to assess the relative proportion of each source comprehensively. ArcMap 10.8 was utilized to investigate land use types and population distribution characteristics in the PRD urban agglomeration, and the regional spatial distribution map was drawn by integrating the raster dataset with a spatial resolution of 10 m, obtained from the Institute of Tibetan Plateau Research, with LandScan population data. IBM SPSS Statistics 26 was utilized for VOC data processing, including correlation and significance analyses of VOCs and meteorological factors across different seasons. Detailed formulas and parameters were provided in SI.

Data availability

All additional data to perform the analyses are available upon reasonable request from the corresponding author (meicheng.wen@gdut.edu.cn).

Received: 26 October 2025; Accepted: 31 January 2026;

Published online: 06 March 2026

References

- Zhou, X., Zhou, X., Wang, C. & Zhou, H. Environmental and human health impacts of volatile organic compounds: a perspective review. *Chemosphere* **313**, 137489 (2023).
- Ciou, Z.-J., Ting, Y.-C., Hung, Y.-L. & Shie, R.-H. Implications of photochemical losses of VOCs: An integrated approach for source apportionment, ozone formation potential and health risk assessment. *Sci. Total Environ.* **958**, 178009 (2025).
- Wang, Z. et al. Quantitative evidence from VOCs source apportionment reveals O₃ control strategies in northern and southern China. *Environ. Int.* **172**, 107786 (2023).
- He, C. Q. et al. The importance of photochemical loss to source analysis and ozone formation potential: Implications from in-situ observations of volatile organic compounds (VOCs) in Guangzhou, China. *Atmos. Environ.* **320**, 120320 (2024).
- Liang, Z. et al. Odorous VOCs released from bio-decomposition and its interaction mechanism with bacteria: Compared inter-type with intra-type household garbage. *J. Clean. Prod.* **447**, 141523 (2024).
- Corteselli, E. & Samet, J. 41-Lipid hydroperoxides as mediators of ozone-induced oxidative changes in human airway epithelial cells. *Free Radical Biol. Med.* **112**, 42 (2017).
- Zhang, Z., Yao, M., Wu, W., Zhao, X. & Zhang, J. Spatiotemporal assessment of health burden and economic losses attributable to short-term exposure to ground-level ozone during 2015–2018 in China. *BMC Public Health* **21**, 1069 (2021).
- Lu, X. et al. Rapid increases in warm-season surface ozone and resulting health impact in China since 2013. *Environ. Sci. Technol. Lett.* **7**, 240–247 (2020).
- Yang, G., Liu, Y. & Li, X. Spatiotemporal distribution of ground-level ozone in China at a city level. *Sci. Rep.* **10**, 7229 (2020).
- Lu, H., Lyu, X., Cheng, H., Ling, Z. & Guo, H. Overview on the spatial-temporal characteristics of the ozone formation regime in China. *Environ. Sci. Proc. Imp.* **21**, 916–929 (2019).
- Xie, Y. et al. Comparison of health and economic impacts of PM_{2.5} and ozone pollution in China. *Environ. Int.* **130**, 104881 (2019).
- Tadic, I. et al. Central role of nitric oxide in ozone production in the upper tropical troposphere over the Atlantic Ocean and western Africa. *Atmos. Chem. Phys.* **21**, 8195–8211 (2021).
- Liu, B. et al. Effect of photochemical losses of ambient volatile organic compounds on their source apportionment. *Environ. Int.* **172**, 107766 (2023).
- Coggon, M. M. et al. Volatile chemical product emissions enhance ozone and modulate urban chemistry. *Proc. Natl. Acad. Sci. USA* **118**, e2026653118 (2021).
- Carter, W. P. L. Development of the SAPRC-07 chemical mechanism. *Atmos. Environ.* **44**, 5324–5335 (2010).
- Zou, Y. et al. Source apportionment and ozone formation mechanism of VOCs considering photochemical loss in Guangzhou, China. *Sci. Total Environ.* **903**, 166191 (2023).
- Wang, W. et al. Direct observations indicate photodegradable oxygenated volatile organic compounds (OVOCs) as larger contributors to radicals and ozone production in the atmosphere. *Atmos. Chem. Phys.* **22**, 4117–4128 (2022).
- Deng, W. et al. Atmospheric occurrences and health risk assessment of polycyclic aromatic hydrocarbons and their derivatives in a typical coking facility and surrounding areas. *Chemosphere* **341**, 139994 (2023).
- Xiong, Y., Huang, Y. & Du, K. Health risk-oriented source apportionment of hazardous volatile organic compounds in eight Canadian cities and implications for prioritizing mitigation strategies. *Environ. Sci. Technol.* **56**, 12077–12085 (2022).
- Julien, M. et al. Intramolecular ¹³C isotope distributions of butane from natural gases. *Chem. Geol.* **541**, 119571 (2020).
- Meng, Y. et al. Ambient volatile organic compounds at a receptor site in the Pearl River Delta region: Variations, source apportionment and effects on ozone formation. *J. Environ. Sci.* **111**, 104–117 (2022).
- Wang, W. et al. Volatile organic compound emissions from typical industries: Implications for the importance of oxygenated volatile organic compounds. *Atmos. Pollut. Res.* **14**, 101640 (2023).
- Lee, J. et al. Pollution characteristics and secondary formation potential of volatile organic compounds in the multi-industrial city of Ulsan, Korea. *Atmos. Environ.* **319**, 120313 (2024).
- Cao, L. et al. Significance of volatile organic compounds to secondary pollution formation and health risks observed during a summer campaign in an industrial urban area. *Toxics* **12**, 34 (2024).
- Mozaffar, A. et al. Measurement report: High contributions of halocarbon and aromatic compounds to atmospheric volatile organic compounds in an industrial area. *Atmos. Chem. Phys.* **21**, 18087–18099 (2021).
- Ning, G. et al. Impact of low-pressure systems on winter heavy air pollution in the northwest Sichuan Basin, China. *Atmos. Chem. Phys.* **18**, 13601–13615 (2018).
- Ryu, Y. H. & Min, S. K. Leveraging physics-based and explainable machine learning approaches to quantify the relative contributions of rain and air pollutants to wet deposition. *Sci. Total Environ.* **931**, 172980 (2024).
- Gomes Alves, E. et al. Intra- and interannual changes in isoprene emission from central Amazonia. *Atmos. Chem. Phys.* **23**, 8149–8168 (2023).
- Cui, L. et al. Enhanced dataset of global marine isoprene emissions from biogenic and photochemical processes for the period 2001–2020. *Earth Syst. Sci. Data* **15**, 5403–5425 (2023).
- Qi, Y., Chen, H. & Zhu, S. Impacts of land–atmosphere coupling on summer extreme hot-humid compound events over Southern Eurasia under different sea surface temperature backgrounds. *Adv. Atmos. Sci.* **42**, 744–760 (2025).
- Wu, W., Deng, W. & Zhu, L. *Source Analysis and Distribution of Atmospheric VOCs in Nanchang, China (in Chinese)*. (Nanchang University, 2024).
- Somekh, M., Iron, M. A., Khenkin, A. M. & Neumann, R. The formylxyl radical: electrophilicity, C–H bond activation and anti-Markovnikov selectivity in the oxidation of aliphatic alkenes. *Chem. Sci.* **11**, 11584–11591 (2020).
- Wu, Y. et al. Changes in source apportioned VOCs during high O₃ periods using initial VOC–concentration–dispersion normalized PMF. *Sci. Total Environ.* **896**, 165182 (2023).
- Li, S. et al. Evolution of source attributed organic aerosols and gases in a megacity of central China. *Atmos. Chem. Phys.* **22**, 6937–6951 (2022).
- Shaw, J. T. et al. A self-consistent, multivariate method for the determination of gas-phase rate coefficients, applied to reactions of atmospheric VOCs and the hydroxyl radical. *Atmos. Chem. Phys.* **18**, 4039–4054 (2018).
- Berg, F. et al. Temperature-dependent rate coefficients for the reactions of OH radicals with selected alkanes, aromatic compounds, and monoterpenes. *Atmos. Chem. Phys.* **24**, 13715–13731 (2024).
- Wu, Y. et al. Tracing the formation of secondary aerosols influenced by solar radiation and relative humidity in suburban environment. *J. Geophys. Res.-Atmos.* **127**, e2022JD036913 (2022).
- Gómez Alvarez, E. et al. Unexpectedly high indoor hydroxyl radical concentrations associated with nitrous acid. *Proc. Natl. Acad. Sci. USA* **110**, 13294–13299 (2013).
- Xie, G. et al. Compositions, sources, and potential health risks of volatile organic compounds in the heavily polluted rural North China Plain during the heating season. *Sci. Total Environ.* **789**, 147956 (2021).
- Harrison, R. M., Vu, T. V., Jafar, H. & Shi, Z. More mileage in reducing urban air pollution from road traffic. *Environ. Int.* **149**, 106329 (2021).

41. Liu, C. & Shi, K. A review on methodology in O₃-NO_x-VOC sensitivity study. *Environ. Pollut.* **291**, 118249 (2021).
42. Wang, B. et al. Variation of ambient non-methane hydrocarbons in Beijing city in summer 2008. *Atmos. Chem. Phys.* **10**, 5911–5923 (2010).
43. Deng, W. et al. Atmospheric occurrences and bioavailability health risk of PAHs and their derivatives surrounding a non-ferrous metal smelting plant. *J. Hazard. Mater.* **470**, 134200 (2024).
44. Li, C. et al. Divergent summertime surface O₃ pollution formation mechanisms in two typical Chinese cities in the Beijing-Tianjin-Hebei region and Fenwei Plain. *Sci. Total Environ.* **870**, 161868 (2023).
45. Mumby, S., Chung, K. F. & Adcock, I. M. Transcriptional effects of ozone and impact on airway inflammation. *Front. Immunol.* **10**, 1610 (2019).
46. Yin, H., Pizzol, M. & Xu, L. External costs of PM_{2.5} pollution in Beijing, China: uncertainty analysis of multiple health impacts and costs. *Environ. Pollut.* **226**, 356–369 (2017).
47. Awuor, L. & Melles, S. The influence of environmental and health indicators on premature mortality: an empirical analysis of the City of Toronto's 140 neighborhoods. *Health Place* **58**, 102155 (2019).
48. Ramírez, N., Cuadras, A., Rovira, E., Borrull, F. & Marcé, R. M. Chronic risk assessment of exposure to volatile organic compounds in the atmosphere near the largest Mediterranean industrial site. *Environ. Int.* **39**, 200–209 (2012).
49. Wen, M. et al. Atmospheric VOCs in an industrial coking facility and the surrounding area: characteristics, spatial distribution and source apportionment. *J. Environ. Sci.* **138**, 660–670 (2024).
50. Gao, J. et al. Comparative study of volatile organic compounds in ambient air using observed mixing ratios and initial mixing ratios taking chemical loss into account—a case study in a typical urban area in Beijing. *Sci. Total Environ.* **628–629**, 791–804 (2018).
51. Wu, Y. et al. Source apportionment of VOCs based on photochemical loss in summer at a suburban site in Beijing. *Atmos. Environ.* **293**, 119459 (2023).
52. Sahu, L. K. et al. Impact of COVID-19 pandemic lockdown in ambient concentrations of aromatic volatile organic compounds in a metropolitan city of western India. *J. Geophys. Res-Atmos.* **27**, 127 (2022).
53. Xu, M. et al. Spatiotemporal analysis of particulate air pollution and ischemic heart disease mortality in Beijing, China. *Environ. Health* **13**, 109 (2014).
54. Vicedo-Cabrera, A. M. et al. Short term association between ozone and mortality: global two stage time series study in 406 locations in 20 countries. *BMJ* **368**, m108 (2020).
55. Burnett, R. T. et al. An integrated risk function for estimating the global burden of disease attributable to ambient fine particulate matter exposure. *Environ. Health Persp.* **122**, 397–403 (2014).
56. Cao, C. et al. Estimating the value of a statistical life in China: A contingent valuation study in six representative cities. *Chin. J. Popul. Resou. Environ.* **21**, 269–278 (2023).
57. OECD. *The Cost of Air Pollution: Health Impacts of Road Transport*. (OECD Publishing, 2014).

Acknowledgements

This study was financially supported by Guangdong Provincial Natural Science Fund for Distinguished Young Scholars (2022B1515020051 and 2022B1515020062), National Natural Science Foundation of China (42377364, 42077332 and 42577034), Science and Technology Program of Guangzhou, China (2025A04J5187).

Author contributions

W.D.: methodology, investigation, resources, writing-original draft, data curation, formal analysis. L.W.: formal analysis, data curation. J.H.: methodology, data curation. Z.G. and J.Y.: data curation. J.X.: methodology, validation. H.L.: methodology, validation. M.W.: writing-reviewing and editing, formal analysis, supervision, and funding acquisition.

Competing interests

The authors declare no competing interests.

Additional information

Supplementary information The online version contains supplementary material available at <https://doi.org/10.1038/s44407-026-00055-8>.

Correspondence and requests for materials should be addressed to Meicheng Wen.

Reprints and permissions information is available at <http://www.nature.com/reprints>

Publisher's note Springer Nature remains neutral with regard to jurisdictional claims in published maps and institutional affiliations.

Open Access This article is licensed under a Creative Commons Attribution 4.0 International License, which permits use, sharing, adaptation, distribution and reproduction in any medium or format, as long as you give appropriate credit to the original author(s) and the source, provide a link to the Creative Commons licence, and indicate if changes were made. The images or other third party material in this article are included in the article's Creative Commons licence, unless indicated otherwise in a credit line to the material. If material is not included in the article's Creative Commons licence and your intended use is not permitted by statutory regulation or exceeds the permitted use, you will need to obtain permission directly from the copyright holder. To view a copy of this licence, visit <http://creativecommons.org/licenses/by/4.0/>.

© The Author(s) 2026